

Preparing for InSight: Evaluation of the Blind Test for Martian Seismicity

by Martin van Driel, Savas Ceylan, John Francis Clinton, Domenico Giardini, Hector Alemany, Amir Allam, David Ambrois, Julien Balestra, Bruce Banerdt, Dirk Becker, Maren Böse, Marc S. Boxberg, Nienke Brinkman, Titus Casademont, Jérôme Chèze, Ingrid Daubar, Anne Deschamps, Fabian Dethof, Manuel Ditz, Melanie Drilleau, David Essing, Fabian Euchner, Benjamin Fernando, Raphael Garcia, Thomas Garth, Harriet Godwin, Matthew P. Golombek, Katharina Grunert, Celine Hadziioannou, Claudia Haindl, Conny Hammer, Isabell Hochfeld, Kasra Hosseini, Hao Hu, Sharon Kedar, Balthasar Kenda, Amir Khan, Tabea Kilchling, Brigitte Knapmeyer-Endrun, Andre Lamert, Jiaxuan Li, Philippe Lognonné, Sarah Mader, Lorenz Marten, Franziska Mehrkens, Diego Mercerat, David Mimoun, Thomas Möller, Naomi Murdoch, Paul Neumann, Robert Neurath, Marcel Paffrath, Mark P. Panning, Fabrice Peix, Ludovic Perrin, Lucie Rolland, Martin Schimmel, Christoph Schröer, Aymeric Spiga, Simon Christian Stähler, René Steinmann, Eleonore Stutzmann, Alexandre Szenicer, Noah Trumpik, Maria Tsekhmistrenko, Cédric Twardzik, Renee Weber, Philipp Werdenbach-Jarklowski, Shane Zhang, and Yingcai Zheng

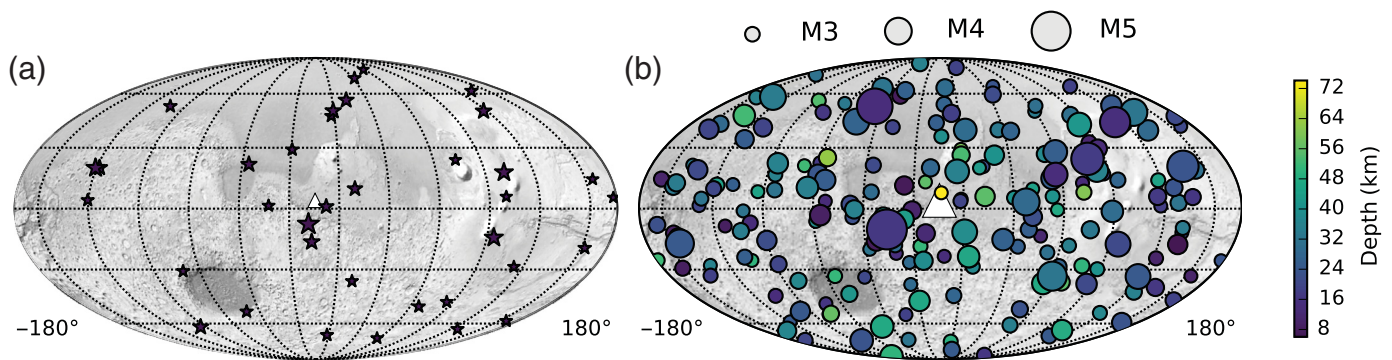
ABSTRACT

In December 2018, the National Aeronautics and Space Administration (NASA) Interior exploration using Seismic Investigations, Geodesy and Heat Transport (InSight) mission deployed a seismometer on the surface of Mars. In preparation for the data analysis, in July 2017, the marsquake service initiated a blind test in which participants were asked to detect and characterize seismicity embedded in a one Earth year long synthetic data set of continuous waveforms. Synthetic data were computed for a single station, mimicking the streams that will be available from InSight as well as the expected tectonic and impact seismicity, and noise conditions on Mars (Clinton *et al.*, 2017). In total, 84 teams from 20 countries registered for the blind test and 11 of them submitted their results in early 2018. The collection of documentations, methods, ideas, and codes submitted by the participants exceeds 100 pages. The teams proposed well established as well as novel methods to tackle the challenging target of building a global seismicity catalog using a single station. This article summarizes the

performance of the teams and highlights the most successful contributions.

INTRODUCTION

The National Aeronautics and Space Administration (NASA) discovery-class mission (Interior exploration using Seismic Investigations, Geodesy and Heat Transport [InSight], Banerdt *et al.*, 2013, see [Data and Resources](#)) to Mars was launched on 5 May 2018 and landed successfully on 26 November. It is dedicated to determining the constitution and interior structure of Mars. For this purpose, InSight deployed a single seismic station with both broadband and short-period seismometers on the surface of Mars, together with a number of other geophysical (Folkner *et al.*, 2018; Spohn *et al.*, 2018) and meteorological (Spiga *et al.*, 2018) sensors. The seismic instrument package (SEIS) is specifically designed for



▲ Figure 1. Catalog summary maps: (a) distribution of impacts and (b) marsquakes in the true catalog, both randomly distributed over the sphere. The maps are centered on the InSight landing site (white triangle). Only a fraction of these events were detectable above the noise level. InSight, Interior exploration using Seismic Investigations, Geodesy and Heat Transport.

Martian conditions to record marsquakes as well as meteoroid impacts and transmits data back to Earth for analysis (Lognonné *et al.*, 2019, see [Data and Resources](#)).

The marsquake service (MQS, Clinton *et al.*, 2018) is tasked with the prompt review, detection, and location of all Martian seismicity recorded by InSight. It will also manage the seismicity catalog, refining locations using the best available Mars models as they are developed during the project. To prepare the InSight science team and the wider seismological community for the data return, the MQS sent an open invitation to participate in a blind test to detect and locate seismic events hidden in a synthetic data set, which was published in *SRL* in July 2017 (Clinton *et al.*, 2017). The data set was made in August 2017 with mandatory registration (available at blind test URL in [Data and Resources](#)). Following the submission deadline in February 2018, the true model and event catalog together with the original waveform data are now openly available online.

Purpose of the Test

The blind test was initiated with the main purpose of improving and extending the set of methods for event location, discrimination, and magnitude estimation as well as phase identification and source inversion to be applied in routine analysis of the InSight data set by collecting ideas from outside the InSight science team. It also helped raise the profile of the InSight mission and to familiarize interested scientists with the data set to be expected from Mars.

Beyond this, the test also initiated a major effort to generate a single, consistent, temporal, synthetic data set that collected all best prelanding estimates of seismicity, impacts, synthetic seismograms, atmospheric pressure variations and related noise, instrument self-noise, and 1D structure models. The data set was made available in the same formats, and using similar webservices as are now available for the real data from Mars. For this reason, the data set was also used for various operational readiness tests (ORTs) as well as scientific testing purposes in preparation for data return.

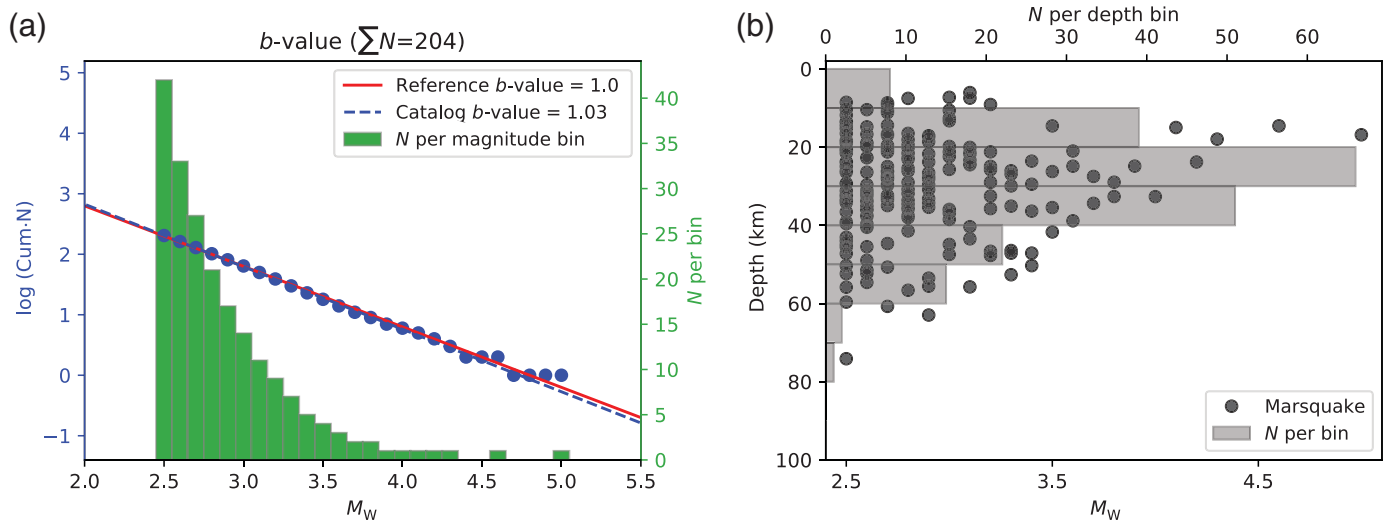
Furthermore, the submitted catalogs allow to derive detection and location thresholds as a function of magnitude and distance that are not based on simple signal-to-noise ratio assumptions, but include the whole complexity of identifying and locating events in the time series. It is important that this data set included randomly distributed events over the sphere. Compared with the global fault distribution (Knapmeyer *et al.*, 2006), this model may have too many events near the landing site, so the total number of detectable events in this data set may be higher than predicted by recent seismicity models of similar total activity (Plesa *et al.*, 2018). This needs to be accounted for if the detection threshold determined in this test is used for constraining seismic activity rates.

In the invitation, we envisioned a quantitative scoring in different categories (event detection and localization accuracy in different magnitude classes, impact discrimination, and focal mechanism), but this turned not to be feasible given the heterogeneity of the submissions and relatively small number of detectable events in the data. Instead, we decided to focus on visual comparisons of the performances and compare them to the level 1 (L1) requirements of the mission, that is, the required accuracy to achieve InSight’s science objectives. The L1 requirements for marsquake location are 25% in distance and 20° in azimuth (Banerdt *et al.*, 2013).

Overview of the Test Data Set

The event catalog included a total of 204 tectonic marsquakes as well as 36 impacts (Fig. 1), with only a fraction of them producing seismic signals above the noise level. The events were randomly distributed over the whole planet where the depth distribution of tectonic events followed a skewed Gaussian distribution with a maximum allowed depth of 80 km. The maximum event size was M_w 5 and the magnitude–frequency distribution approximates a Gutenberg–Richter distribution with $a = 4.88$, $b = 1$; events with $M_w < 2.5$ were neglected (see Fig. 2 and Ceylan *et al.*, 2017).

The impact catalog is based on Teanby (2015) and the size distribution of observed newly dated craters (Daubar *et al.*, 2018), again assuming a globally random distribution. To



▲ **Figure 2.** Statistics for marsquakes in the true catalog. (a) The magnitude–frequency distribution approximates a Gutenberg–Richter distribution with b -value 1.0. The largest event in the catalog has a magnitude M_w 5.0. (b) The magnitude–depth distribution of the marsquakes in the true catalog is a skewed Gaussian with a maximum event number around 20 km and maximum allowed event depth of 80 km.

restrict amplitudes to levels similar to M_w 2.5 events, we only include impacts with impactor mass larger than 100 kg and assume an impact velocity of 10 km/s.

The seismic signals were computed using axisymmetric spectral element method (AxiSEM, Nissen-Meyer *et al.*, 2014) and Instaseis (van Driel *et al.*, 2015) as solutions to the elastic-wave equation in radially symmetric planet models. Continuous time series were then created by superimposing the event-based data with seismic noise that reflects the pre-landing estimates for the surface installed instruments at the landing site (Kenda *et al.*, 2017; Mimoun *et al.*, 2017; Murdoch, Kenda, *et al.*, 2017; Murdoch, Mimoun, *et al.*, 2017). It includes noise generated by the sensors and systems themselves, as well as through sources in Martian environment (such as fluctuating pressure-induced ground deformation, the magnetic field, and temperature-related noise) and nearby lander (such as wind-induced solar panel vibrations).

Synthetic data were generated from one of the 14 candidate models (Zharkov and Gudkova, 2005; Rivoldini *et al.*, 2011; Khan *et al.*, 2016), which were published as part of the data set, but the model choice was not revealed to participants. The model used for creation of waveform data set is shown in Figure 3, which explains two prominent features observed by most participating teams: (1) clear S -wave arrivals were absent in most events due to the low-velocity region in the upper mantle, which made distance estimations based only on relative P - and S -travel times very difficult and (2) at the same time, the bedrock layer at the surface acted as a wave guide and caused a prominent arrival after the P wave with linear move-out that could be used for estimating locations in this 1D setting (see Fig. 4, for an overview of the most visible events). Such a phase is observed over long distances in specific settings on Earth, such as oceanic crust of constant thickness (e.g., Kennett

and Furumura, 2013), but in this blind test, it should be considered an artifact from the simple 1D model. It is not expected to be observed as a global phenomenon on Mars due to attenuation from 3D scattering.

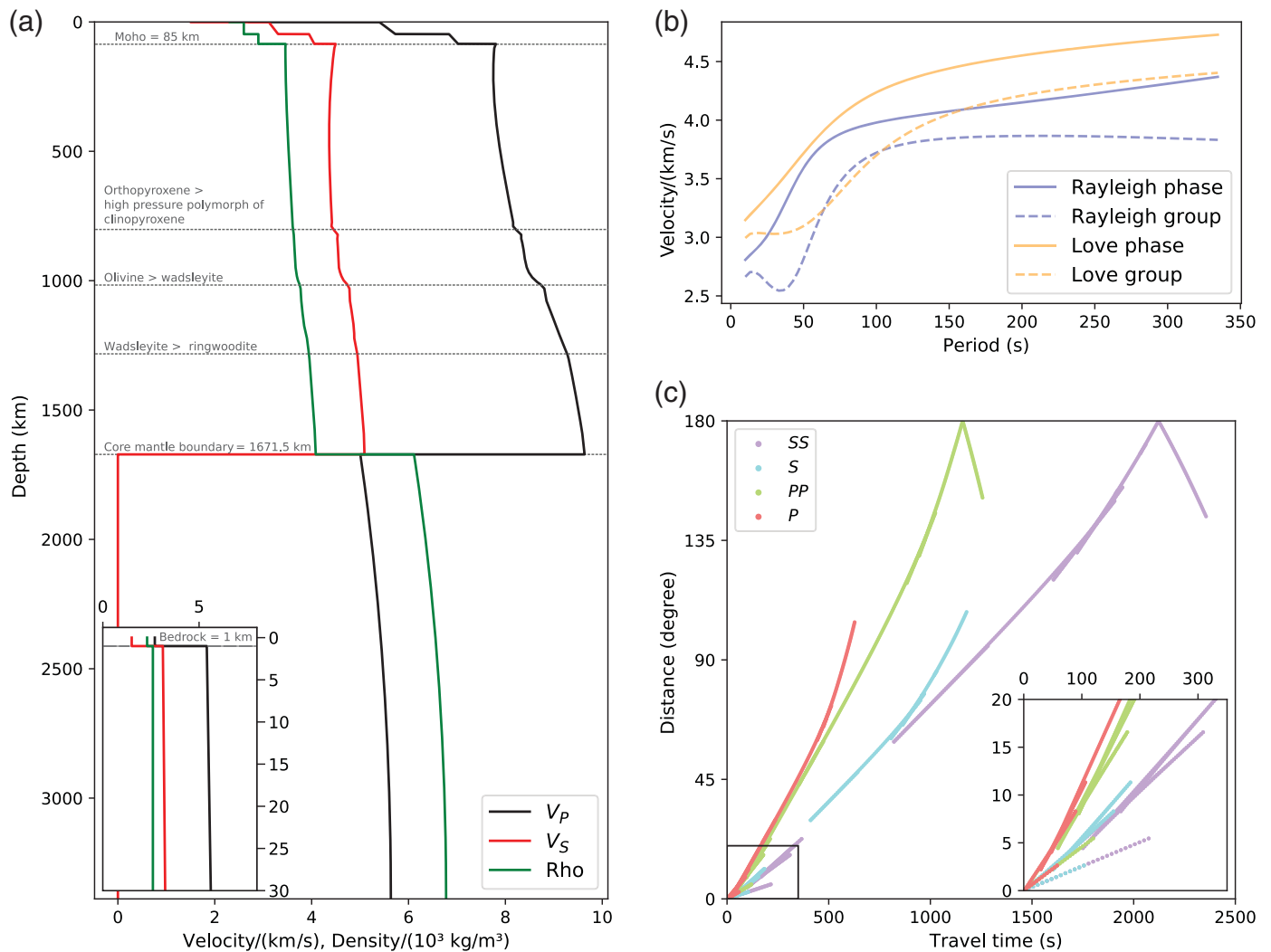
An overview of responsibilities for the generation of the data set can be found in Table 1; further details can be found in Clinton *et al.* (2017). Based on the experience gained and performance of the MQS in particular within this test, the MQS is currently refining the location strategies and running an ORT with synthetic data computed in a 3D model.

In the following sections, we first summarize the methods used by each team. Then, we compare the success of each submission in terms of event detection, as well as estimated event distance, back azimuth, and origin time against the true event parameters.

PARTICIPATION AND METHODS

To ensure effective communication with participants or anyone who wanted to experiment, registration for the test was mandatory for accessing the data set. On the other hand, participation was completely voluntary; but we strongly encouraged all registrants to submit their results, particularly with event catalogs. In total, 84 teams registered and 11 of them submitted their analysis. Because of the lack of feedback, we do not have a further overview on how test data were used by other teams that downloaded the data but chose not to participate.

The participating teams were composed of researchers both from inside (Institut de Physique du Globe de Paris [IPGP], MQS, and Max Planck) and outside (Colorado, Geazur, Houston, and Utah) the InSight science team. Participant profiles were rather diverse including senior researchers as well as



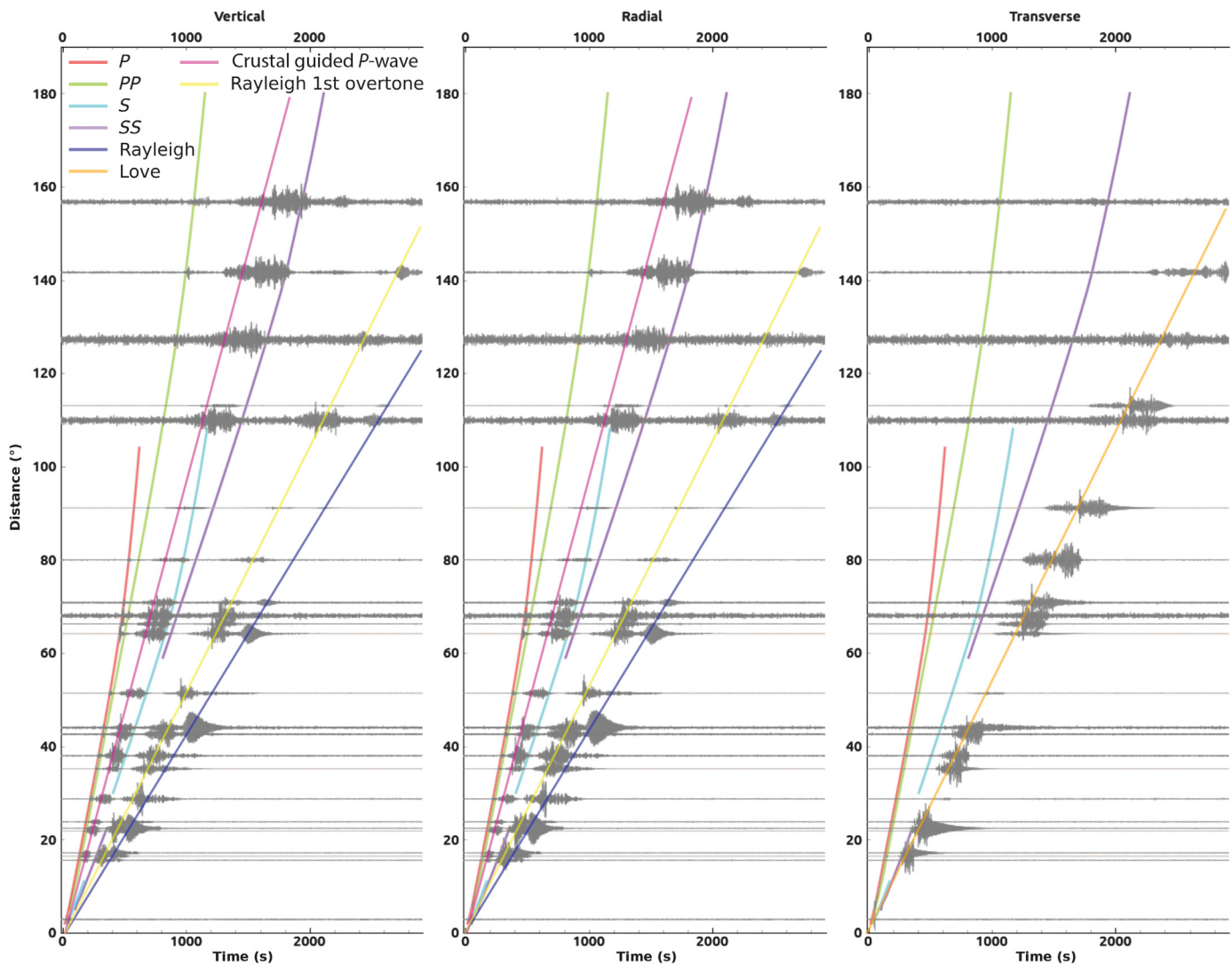
▲ **Figure 3.** Summary of the model EH45TcoldCrust1b that was used in the blind test. Vertical profile of (a) seismic velocities and density, (b) dispersion curves, and (c) travel times. This model includes a low-velocity zone (LVZ, a region with a negative velocity gradient for either or both P and S). The LVZ leads to broad shadow zones for direct-arriving S phases as indicated by gaps in the travel-time curves in (c).

Ph.D. (Bochum, Oxford), masters (Hamburg), and even high school students (SEISonMars@school). Table 2 shows a list of the teams and their members. In Table 3, we summarize the wealth of methods used by the participants with references to previous publications as much as possible, but a significant fraction of the methods applied by participants appears to have been developed specifically for this test.

Most teams inspected the waveforms visually or used spectrograms for event detection, whereas four teams (Bochum, Geoazur, Hamburg, and Utah) also utilized short-term average/long-term average (STA/LTA) algorithms with manual review for this purpose. In the case of a single station, event distance can be estimated using relative travel times between different body- and surface waves, and multiorbit surface waves for the larger events. Although the latter is independent of the model (Panning *et al.*, 2017), body and minor arc surface-wave travel times need a reference model for distance estimation. Hence, most teams tried to first determine the model from

the 14 candidate models and then computed locations for that model. Three teams (Bochum, Colorado, and MQS), however, used probabilistic methods to account for the inherent trade-off between model and distance. Combining the distance estimate with the back azimuths of the event and the known station location, an absolute location can be derived. The participants used a large variety of both P and Rayleigh polarization analysis methods for this purpose. Only two teams (Houston and MQS) attempted to determine depth, which was difficult because most events did not show clear depth phases.

Only one team (Colorado) attempted to decorrelate the atmospheric pressure signals to reduce the noise; and another team (Hamburg) classified pressure events automatically, whereas others relied on a visual check to exclude those from the catalog. The Houston team was the only group to derive surface-wave phase velocities. Two teams did not submit a catalog but applied methods that facilitate event detection and phase recognition: IPGP focused on crustal structure and



▲ **Figure 4.** The most visible events in the data set, plotted as a function of distance from the station. Travel-time curves for the most prominent phases are shown in the legend. The waveforms are band-pass filtered between 1.5 and 10 s.

Table 1
Contributions to the Blind Test Data Set

Contribution	Responsible Coauthors (Alphabetically Ordered by Last Names)
Marsquake catalog	Savas Ceylan, John Clinton, and Martin van Driel
Impact catalog	Ingrid Daubar and Matthew P. Golombek
Synthetic seismograms	Martin van Driel and Melanie Drilleau
Synthetic noise and pressure	Melanie Drilleau, Raphael Garcia, Balthasar Kenda, Philippe Lognonné, David Mimoun, Naomi Murdoch, Ludovic Perrin, and Aymeric Spiga
Compilation of 1D models	Amir Khan and Mark P. Panning
Compilation of the data set and webservice	Savas Ceylan, Martin van Driel, and Fabian Euchner
Final choice of 1D model and catalogs	Bruce Banerdt and Martin van Driel
Test conception and initiation	Domenico Giardini and Philippe Lognonné

Table 2
Participating Teams and Their Members

Group Name	Team Members (Alphabetically Ordered by Last Names)
Bochum	Marc S. Boxberg, Manuel Ditz, Andre Lamert, Thomas Möller, and Marcel Paffrath
Colorado	Shane Zhang
Geoazur	Hector Alemany, David Ambrois, Julien Balestra, Jérôme Chèze, Anne Deschamps, Diego Mercerat, Fabrice Peix, Lucie Rolland, and Cédric Twardzik
SEISonMars@school	French Seismological Educational Network (SISMOS à l'École) coordinated by Julien Balestra
Hamburg	Dirk Becker, Titus Casademont, Fabian Dethof, David Essing, Katharina Grunert, Celine Hadziioannou, Isabell Hochfeld, Tabea Kilchling, Sarah Mader, Lorenz Marten, Franziska Mehrkens, Paul Neumann, Robert Neurath, Christoph Schröer, René Steinmann, Noah Trumpik, and Philipp Werdenbach-Jarklowski
Houston	Hao Hu, Jiaxuan Li, and Yingcai Zheng
IPGP	Martin Schimmel and Eleonore Stutzmann
Max Planck	Conny Hammer and Brigitte Knapmeyer-Endrun
MQS	Maren Böse, Nienke Brinkman, Savas Ceylan, John Francis Clinton, Fabian Euchner, Domenico Giardini, Sharon Kedar, Amir Khan, and Simon Christian Stähler
Oxford	Benjamin Fernando, Thomas Garth, Harriet Godwin, Claudia Haindl, Kasra Hosseini, Alexandre Szenicer, and Maria Tsekhmistrenko
Utah	Amir Allam

IPGP, Institut de Physique du Globe de Paris; MQS, marsquake service.

polarization analysis rather than event locations and Max Planck implemented a Hidden Markov model (HMM) approach to detect events, which allowed them to provide only event detection times and no origin times.

None of the teams submitted information on the focal mechanisms within this test, but the method of [Stähler and Sigloch \(2014\)](#) has been applied successfully after the submission deadline by the MQS team for the largest three events ([Clinton *et al.*, 2018](#)).

PERFORMANCE

In the blind test announcement ([Clinton *et al.*, 2017](#)), it was stated that it was mandatory to provide a location and origin time. A number of teams were only able to provide approximate detection times without locations and others only provided locations for parts of their catalog. We decided to also show these results, though we understand that other teams that closely followed this rule may have left out detected events that they were not able to locate and hence the detection statistics needs to be interpreted with care.

Figure 5 gives an overview of the performance by different teams in detecting and locating events:

- The blue bars represent the total number of events in each catalog, that besides true and false detections, may also include multiple detections for a single event. This was in particular the case for the fully automatic HMM approach from the Max Planck team, because HMM is fundamentally a pattern matching approach operating on certain statistics that heavily relies on proper classification and representation of training events. In this application, only a single training event was used.

- The orange bars represent the number of events that could be associated with an event in the true catalog solely based on the origin time and with duplicate detections removed. Because we prevented event waveforms from overlapping in the seismicity catalog, the association is straightforward. We assume any event time submitted that occurs within a window from 750 s before and 1500 s after the true origin time as correct. The three teams that performed best in detection (MQS, Hamburg, and Bochum) all relied on a high degree of visual data inspection, whereas two of them (Hamburg and Bochum) assisted by STA/LTA triggering. Comparing seismic and pressure data visually allowed these teams to exclude most nonseismic events. The MQS produced daily spectrograms that were visually scanned by different members of the team, which proved a very effective way to maximize event detection.
- The green bars represent the number of events for which full location information was provided (origin time, distance, and azimuth).
- Finally, the red bars represent events that were located within the InSight mission L1 requirements for location accuracy.

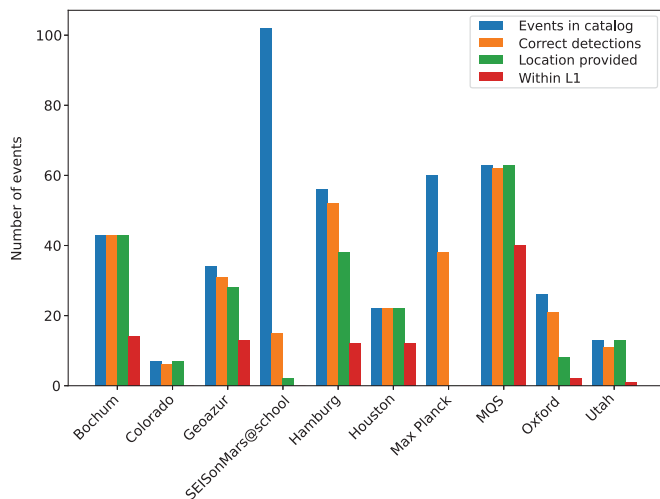
Figure 6 shows a more detailed view of the 10 submitted catalogs, highlighting false detections (blue vertical lines) as well as detection and location of marsquakes (circles) impacts (stars). The rate of correct detection and location as well as false detections varies significantly over the time span of the data set. This may be related to sharing of the workload between multiple operators; for example, the MQS split the initial detection on monthly bases between team members.

In the following, we focus on the six teams that provided the most complete results in terms of the number of events

Table 3
Overview of Participating Teams and Methods Employed

Group Name	Methods
Bochum	<p>Detection: STA/LTA triggering and manual review</p> <p>Location: three probabilistic polarization analysis methods for azimuth (Selby, 2001; Eisermann <i>et al.</i>, 2015); probabilistic body wave and Rayleigh-group travel times for distance (Panning <i>et al.</i>, 2015; Böse <i>et al.</i>, 2016)</p>
Colorado	<p>Detection: manual event detection on band-pass filtered traces</p> <p>Location: probabilistic polarization analysis for azimuth (Böse <i>et al.</i>, 2016); probabilistic body wave and Rayleigh-group travel times for distance (Panning <i>et al.</i>, 2015)</p> <p>Magnitudes: Clinton <i>et al.</i> (2017)</p> <p>Other efforts: attempt of pressure decorrelation (Murdoch, Kenda, <i>et al.</i>, 2017); verification of the methods on synthetics (van Driel <i>et al.</i>, 2015; Ceylan <i>et al.</i>, 2017)</p>
Geoazur	<p>Detection: automated event detection using different STA/LTA triggers, manual classification</p> <p>Location: distance based on relative <i>P</i>-<i>S</i> travel time, azimuth based on <i>P</i> and Rayleigh polarization (Jurkevics, 1988; Bayer <i>et al.</i>, 2012; Panning <i>et al.</i>, 2015; Khan <i>et al.</i>, 2016)</p> <p>Other efforts: correct model chosen based on surface-wave dispersion</p>
SEISonMars@school Hamburg	<p>Detection: visual inspection of the data, manual event detection</p> <p>Detection: visual (data and spectrograms) and automated event detection (STA/LTA triggers with variable parameter settings, spectrogram detector)</p> <p>Location: visual azimuth determination using hodograms; distance based on relative <i>P</i>, <i>S</i>, <i>R1</i>, and multiple orbit surface waves</p> <p>Other efforts: correct model chosen based on travel times and dispersion curves; automated pressure event classification</p>
Houston	<p>Location: Surface-wave polarization for azimuth (Vidale, 1986); relative surface-wave travel times for distance (including minor arc only)</p> <p>Other efforts: high-resolution dispersion analysis of multiorbit surface waves to determine phase velocity and the correct model (Zheng <i>et al.</i>, 2015; Zheng and Hu, 2017); depth based on depth phases</p>
IPGP	<p>Key efforts: autocorrelation to detect crustal discontinuities (Schimmel, 1999; Schimmel, Stutzmann, and Gallart, 2011); degree of polarization Rayleigh-wave detection and azimuth (Schimmel, Stutzmann, <i>et al.</i>, 2011); no catalog submitted</p>
Max Planck	<p>Key efforts: automated event detection and classification using HMMs (Hammer <i>et al.</i>, 2012, 2013; Knapmeyer-Endrun and Hammer, 2015); no catalog submitted</p>
Marsquake service	<p>Detection: event detection by visual screening of spectrograms</p> <p>Location: four probabilistic methods for distance and azimuth for body- and surface waves (Böse <i>et al.</i>, 2016); new model set for probabilistic methods based on the largest events; distances refined by visual alignment of waveforms vs. distance for all events; multiple iterations in relocation to detect outliers</p> <p>Magnitudes: Böse <i>et al.</i> (2018)</p> <p>Other efforts: event classification based on quality of location (Clinton <i>et al.</i>, 2018); correct model chosen; by comparing event waveforms at similar distances, depths were indicated and one event was correctly identified as an impact</p>
Oxford	<p>Detection: visual event detection on band-pass filtered traces</p> <p>Location: differential travel times and surface-wave dispersion for distance; particle motion and polarization for azimuth (three different methods); detailed description in Fernando <i>et al.</i> (2018)</p> <p>Other efforts: three models suggested, including the correct one</p>
Utah	<p>Detection: manual event detection assisted by STA/LTA using multiple filter bands and polarization (Jurkevics, 1988; Allam <i>et al.</i>, 2014; Ross and Ben-Zion, 2014)</p> <p>Location: azimuth based on <i>P</i> and Rayleigh polarization; distance based on relative <i>P</i>- and <i>S</i> travel times</p> <p>Other efforts: model wrongly detected based on H/V ratio (Lin <i>et al.</i>, 2014) and receiver functions (Allam <i>et al.</i>, 2017); event classification based on radial-to-transverse ratio</p>

H/V, horizontal-to-vertical; HMM, Hidden Markov model; IPGP, Institut de Physique du Globe de Paris; STA/LTA, short-term average/long-term average.



▲ **Figure 5.** Summary of the team performances: total number of detected events in the submitted catalogs (blue), detected events that can be associated with an event in the true catalog (orange), detected events in the submitted catalogs with full locations provided (green), and number of these events that lie within L1 mission requirements (red). Note the difference between orange and blue indicates false detections. L1, level 1; MQS, marsquake service.

correctly located within L1 requirements: Bochum, Geoazur, Hamburg, Houston, the MQS, and Oxford. The MQS submitted two catalogs (focusing on absolute and relative distances, respectively), but because they are of very similar quality and were built iteratively using information from both approaches, we treat them as one for the purpose of this article.

Distance–Magnitude Trade-Off

Figure 7 provides an overview of the six most complete catalogs with respect to distance and magnitude. It also reveals that although the MQS had the highest number of correct detections, a handful of events were missed that other teams were able to detect, and some detected events were located more precisely by other teams. The MQS carefully analyzed each of these events again to identify the root cause of these mislocations and unidentified events. Besides mislabeled seismic phases, several issues in the MQS workflow were recognized and resolved, with the most important improvement being the increase of the overlap in the daily plots used for visual screening.

Most of the six teams detected all events above magnitude 4, globally. Between magnitudes 3 and 4, several teams detected all events until approximately 40° distance, even though they could not locate them within the L1 requirements. The MQS detected all events above magnitude 3.5 and all events above magnitude 2.5 within 30° distance, which suggests that the detection threshold may be even lower than 2.5 for regional events. The detection curve for the MQS is only distance and magnitude dependent, without an indication of an effect of different focal mechanisms.

Distance Estimation

Distance estimation (Fig. 8) was complicated by the low-velocity layers in the upper mantle, which made *S* waves very hard to identify in the data with the given noise. An easy estimate based only on the travel-time difference between *P*- and *S* phase could hence not be applied to most events. On the other hand, Rayleigh-wave group arrival times could be used with unrealistically high accuracy in this 1D model, which is one reason for running the current ORT with 3D synthetics. This new test suggests that including estimates of crustal thickness variations from gravity (Wieczorek and Zuber, 2004), topography from Mars Orbiting Laser Altimeter (MOLA), and ellipticity lateral variations of surface-wave arrival times of up to a few hundred seconds should be expected.

An additional simplification was employed by most teams by determining the correct model from the 14 candidate models based on the biggest event in the data set (see Table 3) and then using that model to locate the smaller events. In practice, a number of small events are expected to be seen in the data before any event that is big enough to constrain the model. To add this complexity to the problem, the data in the new 3D test were released in weekly chunks.

The MQS catalog included a data quality classification, in which reliable locations were classified as quality A, unreliable locations as quality B, and very unreliable or unconstrained locations as quality C. Figure 8 indicates that only class C and a few class B events could not be located correctly (Clinton *et al.*, 2018).

Back-Azimuth Estimation

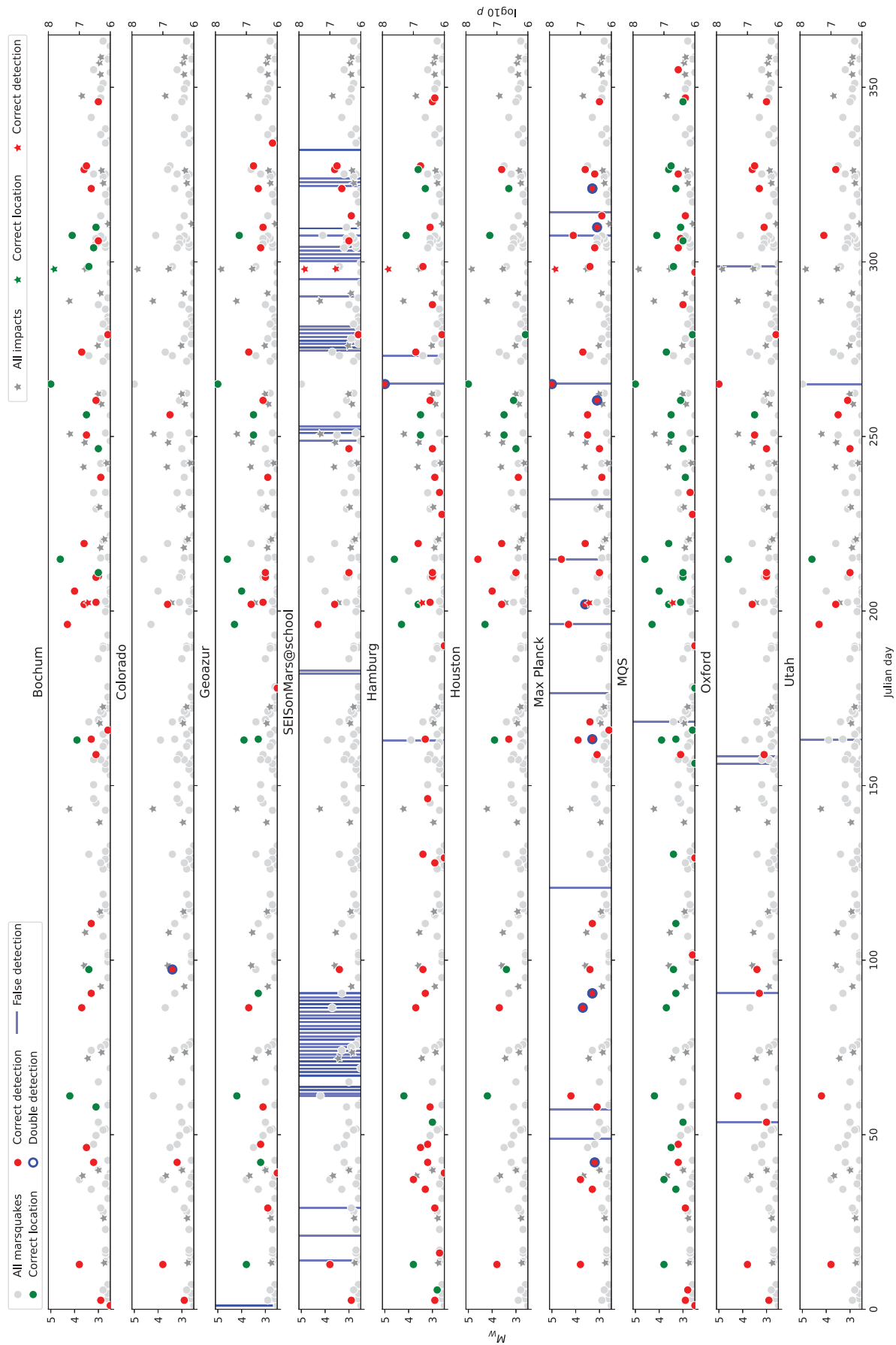
The back-azimuth estimation in Figure 9 reveals that some methods suffer from a 180° ambiguity, which can however be resolved by either assuming retrograde Rayleigh motion or including the incidence angle in *P*-wave azimuth estimates (Panning *et al.*, 2015; Böse *et al.*, 2016). Similar to the distance estimate, all MQS quality A and the majority of quality B location estimates meet the L1 requirement.

Origin Time Estimation

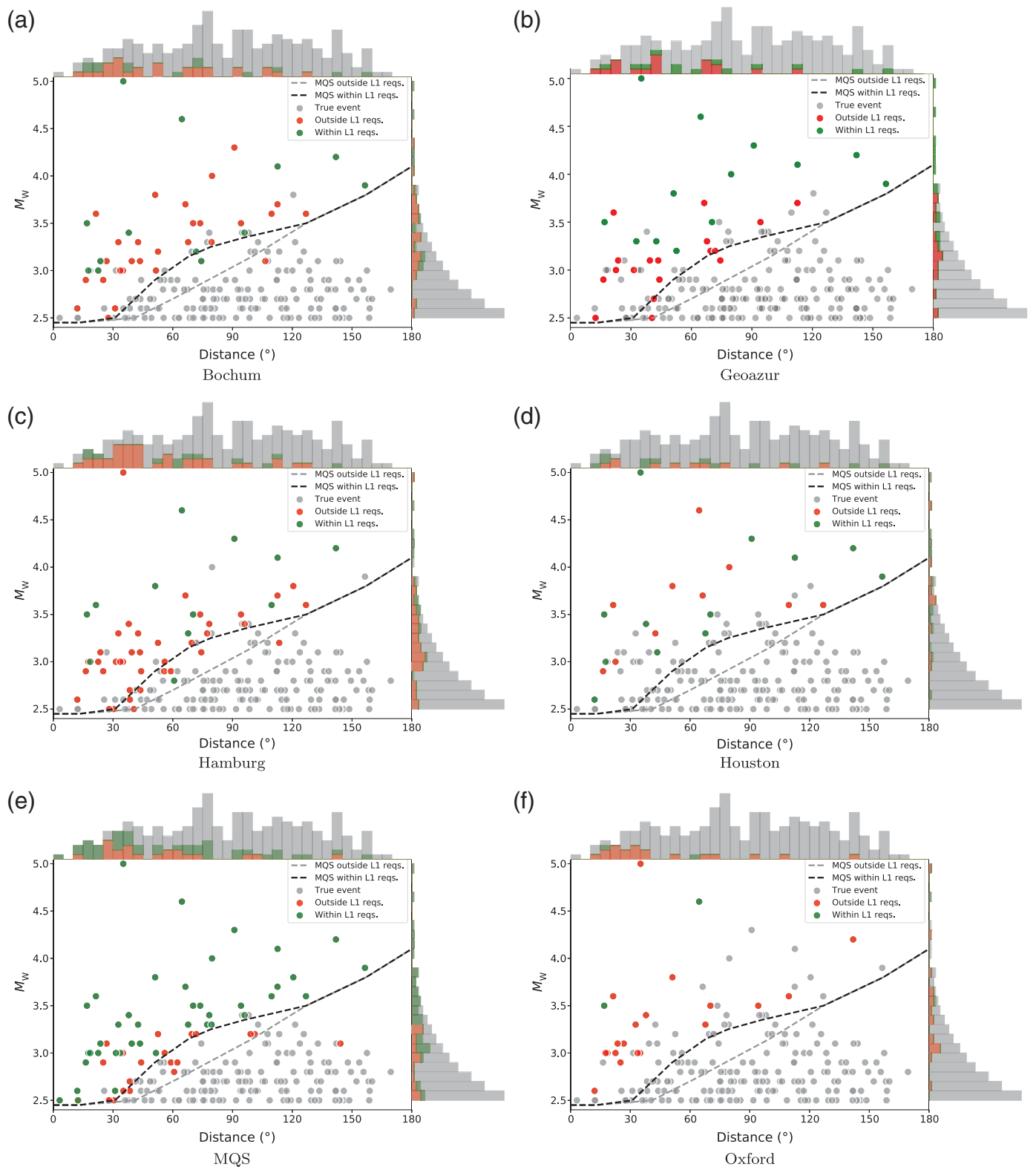
The error in origin time estimation is closely related to distance estimation by the fixed model set that was provided for this test, and this can also be observed in the strong correlation in performance for distance and origin time (Fig. 10). Similar arguments as in the distance estimation apply for the model complexities and 3D effects.

Impact Discrimination

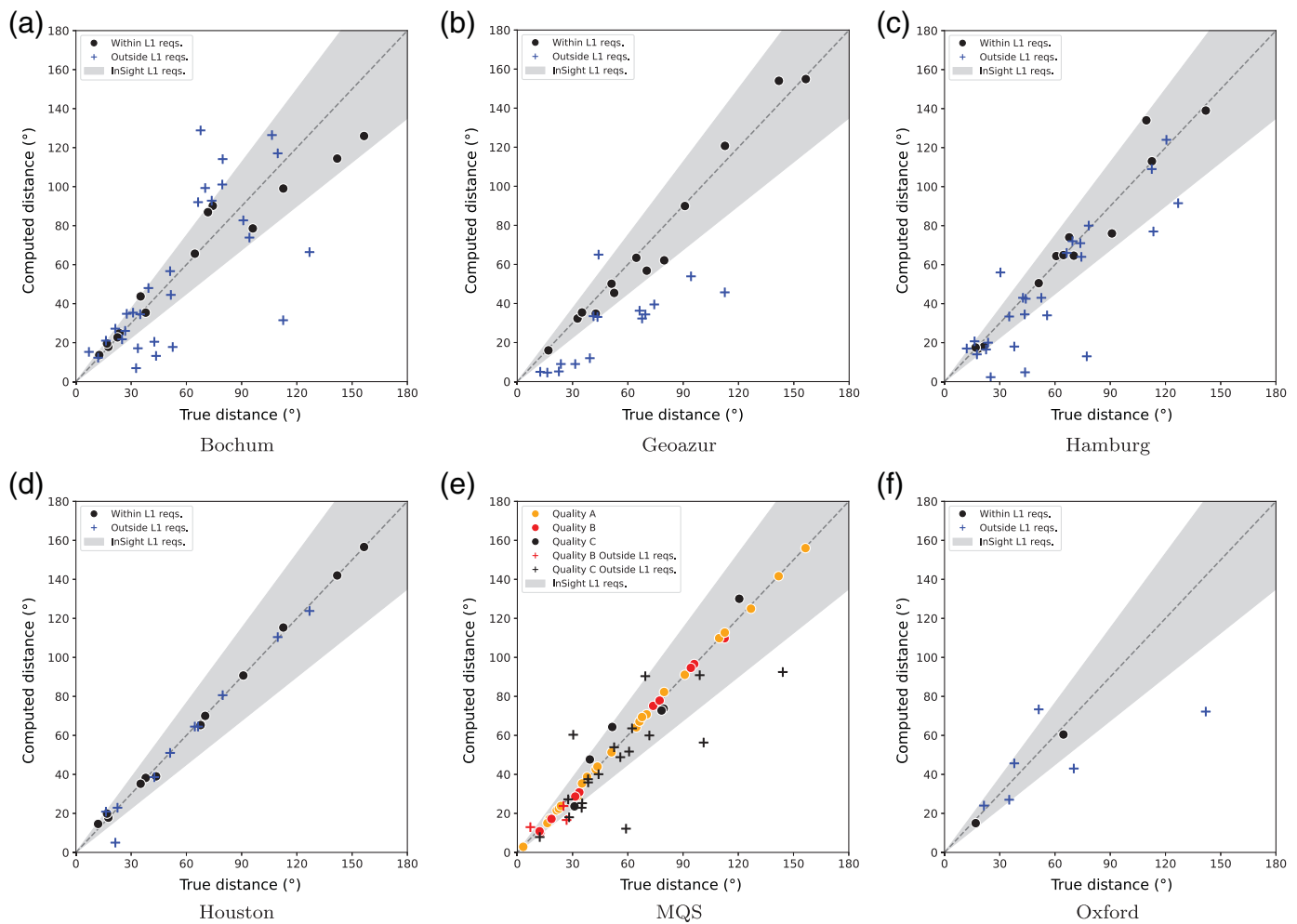
Only one team (MQS) classified the event type as marsquake or impact in their catalog. Only a single event was identified as an impact, which was correct, and no other event was mislabeled as impact. The MQS did miss the biggest impact event of the data set in the detection stage. Hence, we cannot evaluate the distinction capability in this test and just document the three strongest impact events together with three marsquakes for reference in Figure 11. If the signal is above the noise, the waveforms appear very distinct from marsquakes due to



▲ **Figure 6.** Temporal overview of the submitted catalogs indicating correct detections and locations as well as double and false detections. All events in the true catalog are shown, red and green correspond to correct detection and correct location, and those in gray are missing in the submitted catalog. Marsquakes are shown as circles and impacts as stars. Note the scale based on linear momentum p for the impacts on the right side.



▲ **Figure 7.** Distance–magnitude summary for the (a–f) six most complete submitted catalogs. All events in the true catalog are shown for each team, correctly detected in red, correctly located in green, and missed events in gray. The dashed lines approximate the detection threshold (gray dashed line) and correct location threshold (black dashed line) for the MQS. Histograms at the top and right side show the number of correctly detected (red), correctly located (green), and missed events (gray) for a number of distance and magnitude reqs., requirements.



▲ **Figure 8.** Distance performance—comparing the distances provided in the (a–f) six most complete submitted catalogs to the true event distance. Gray area marks the L1 requirement. Note that for an event to be located within L1, we also required correct azimuth and origin time. For the MQS, their data quality classification is indicated. reqs., requirements.

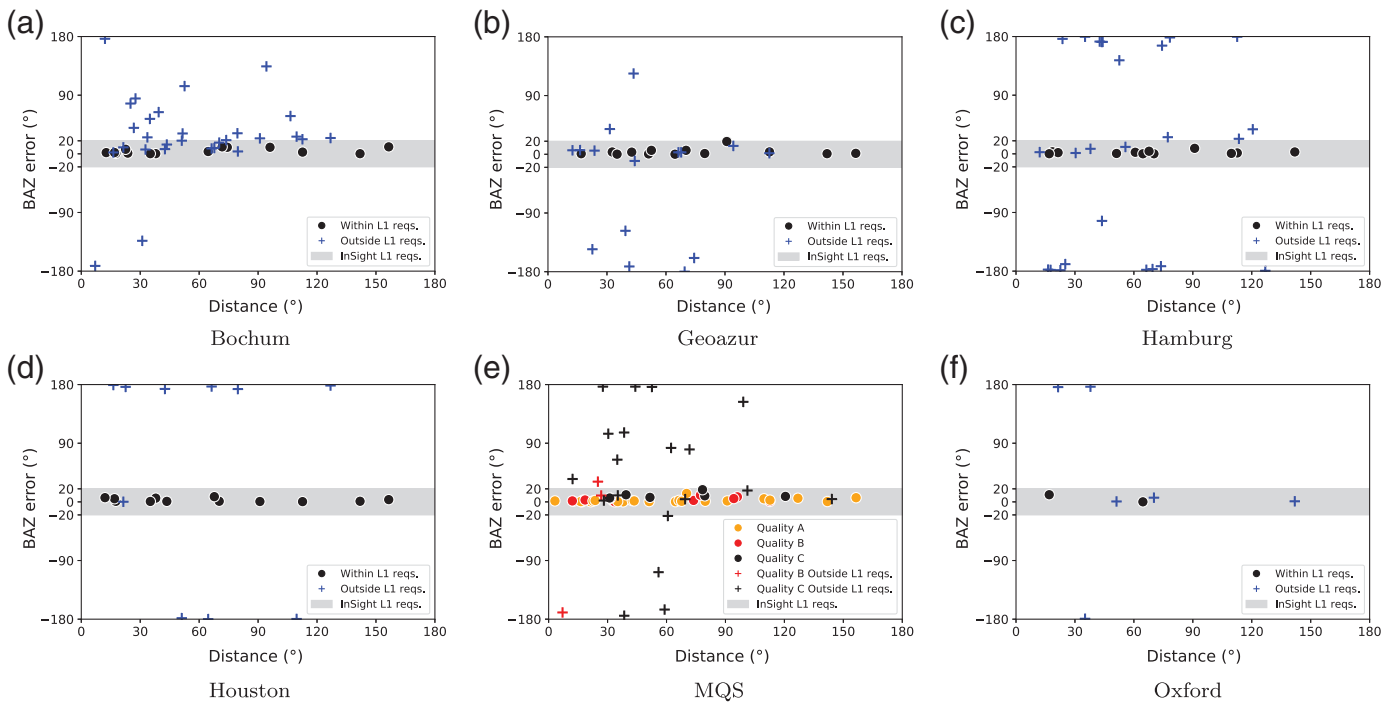
trapped energy in the high quality factor (Q) shallow layers of the 1D model as well as very short-period surface waves excited by the surface source. In contrast, marsquakes at depth neither excite trapped waves in the shallow layers in this 1D model due to Snell's law nor the very short-period surface waves due to their limited penetration depth.

The MQS's classification of the impact was purely based on the waveform's appearance, which they recognized as very different from all other events. With very few impact events ever seismically recorded and the distinct impact behavior due to the atmosphere on Earth compared with the Moon, there is no well-established discrimination technique. [Gudkova et al. \(2011\)](#) suggest a different spectral content of impacts compared with marsquakes for the Moon. Other criteria include the depth of the event, although the absence of depth phases is difficult to demonstrate. In addition, newly detected craters on satellite images from Mars might help to discriminate impact events if they can be correlated in time and location.

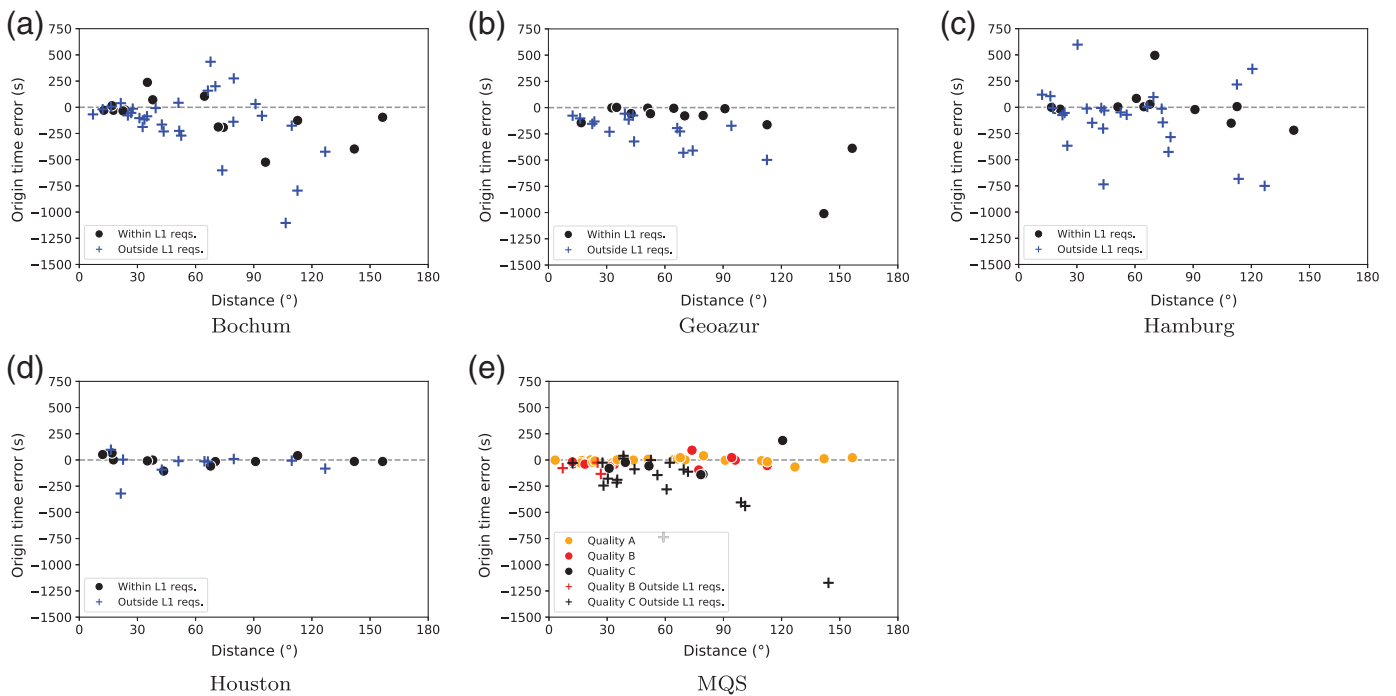
CONCLUSIONS

The submissions to this blind test provided the InSight science team with a range of new ideas and brought the specific challenges of single-station seismology on Mars to a broader range of seismologists from the general community. In practice, the main benefits of the test to the MQS were that it provided the opportunity to thoroughly test software and routines as well as benchmark the event detection and location capabilities on a previously unavailable quality data set, and to evaluate whether there are new or existing methodologies that were overlooked and could significantly improve the MQS's performance.

Finally, various teams contributed to this 1D test with a number of useful and different ideas; however, the algorithms established in the MQS produced comparable or better performance. Further evaluation in the light of the 3D effects from synthetics as well as the actual seismicity observed by the InSight seismometers will be necessary to decide if the MQS

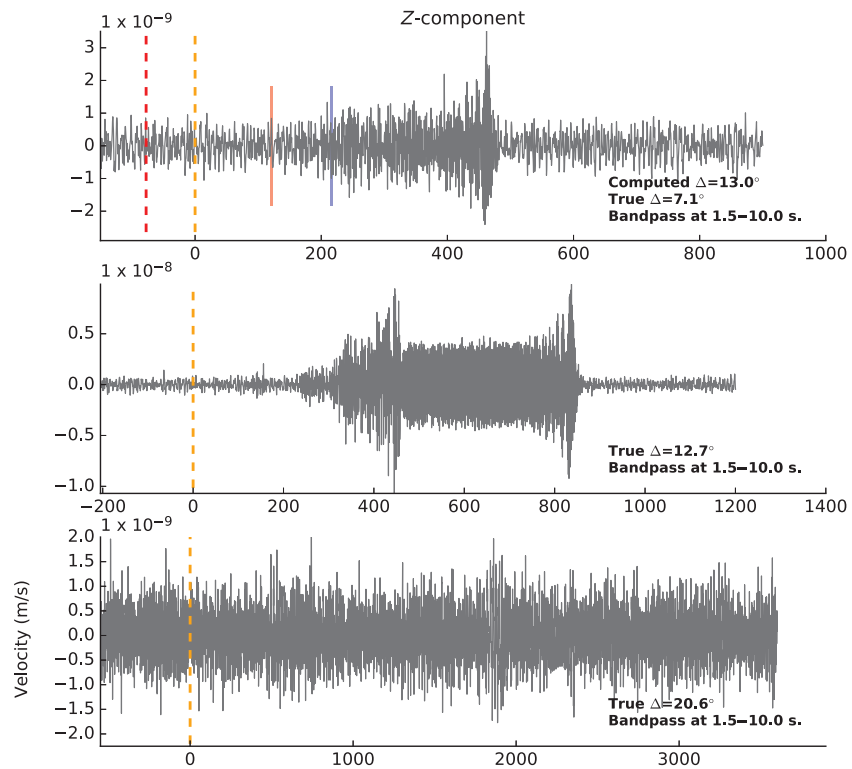
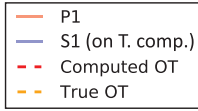
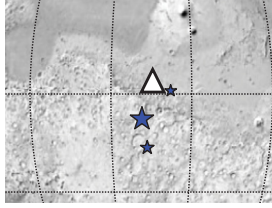


▲ **Figure 9.** Back-azimuth (BAZ) performance for the (a–f) six most complete submitted catalogs in terms of the BAZ estimation error as a function of distance. The gray area marks the mission L1 requirement. Note that for an event to be located within L1, we also required correct distance and origin time. reqs., requirements.

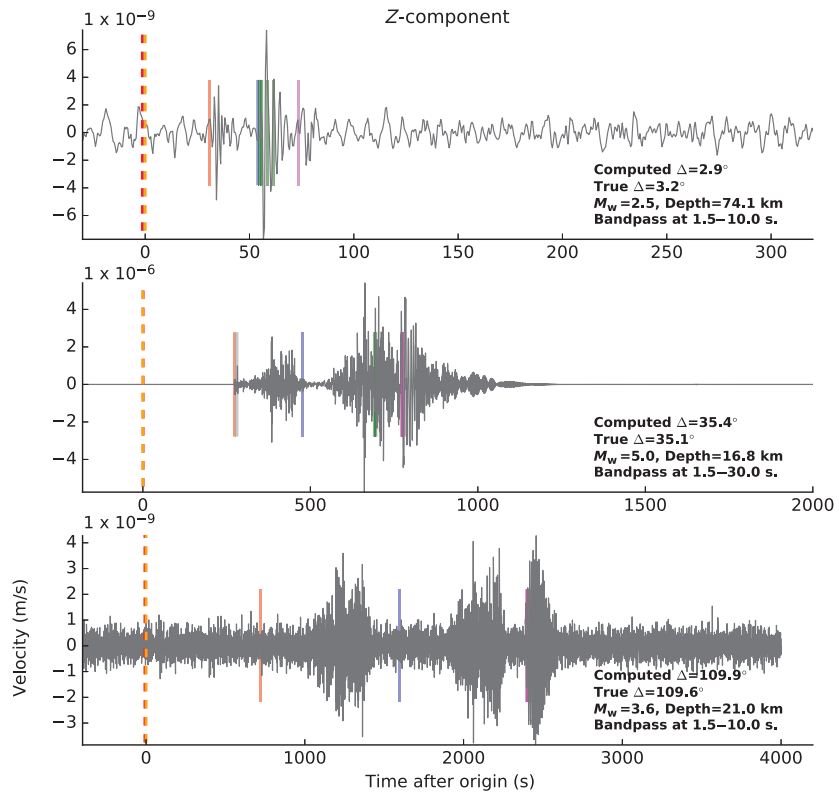
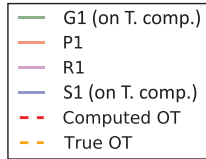
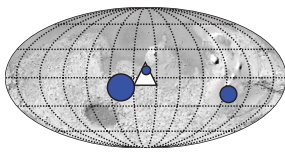


▲ **Figure 10.** Origin time performance for the (a–e) five most complete submitted catalogs in terms of the timing error as a function of distance. Note that there is no L1 requirement, but for an event to be located within L1 we required correct azimuth and distance. Oxford's catalog did not include origin times, but only arrival times; hence, it is omitted here. reqs., requirements.

(a)



(b)



▲ Figure 11. (a) Location and vertical-component waveforms for the three strongest impact signals in the true catalog. On the map, the impacts are indicated by stars (size proportional to the linear momentum), and the station is marked with the triangle. The closest event was correctly identified as an impact by the MQS. Though some other teams identified the largest event, no other team classified it as an impact in their catalogs. (b) Similar plot for three marsquakes for comparison. Seismic phases in both plots are annotated as: S1 and P1, first arriving *S* and *P* wave, in which *S* was only visible on the transverse component (T. comp.); G1 and R1, minor arc Love and Rayleigh waves; OT, source origin time.

will adopt any of the suggested methods from other teams. From the test, it is also obvious that the best performances were produced by the teams that had the time to dedicate to the test—an important lesson for the MQS for organizing routine operations: one team member is always on duty to analyze all new data for possible seismic events with another person as backup. Any suspected event is then analyzed carefully by the review team before communicating to the whole science team (see Clinton *et al.*, 2018, for details on the operations).

The blind test experience helped forming the basis for the currently running ORTs with 3D synthetic data for both the MQS and Mars structure service (Panning *et al.*, 2017), which give an opportunity to the operational teams to train daily data review.

DATA AND RESOURCES

The test data set is described in more detail by Clinton *et al.* (2017) and available online at <http://blindtest.mars.ethz.ch/> (last accessed December 2018). Figures are created using ObsPy (Krischer *et al.*, 2015). Submissions (catalogs and documentation) by individual teams are not publicly available. Interior exploration using Seismic Investigations, Geodesy and Heat Transport (InSight) is available at <http://mars.nasa.gov/insight/> (last accessed May 2019). The seismic instrument package (SEIS) is available at www.seis-insight.eu (last accessed May 2019). ☒

ACKNOWLEDGMENTS

The coauthor list of this article includes contributors to the evaluation (up to and including D. Giardini), contributors to the data set and invitation article (Table 1), as well as the participants of the blind test (Table 2).

This work was jointly funded by Swiss National Science Foundation and French Agence Nationale de la Recherche (SNF-ANR project 157133 “Seismology on Mars”); Swiss State Secretariat for Education, Research and Innovation (project “MarsQuake Service–Preparatory Phase”); and ETH Zürich (project “Preparatory phase for Mars InSight Ground Segment Support”). Additional support came from the Swiss National Supercomputing Centre (CSCS) under Project ID s682. Some of the research described in this article was supported by the Interior exploration using Seismic Investigations, Geodesy and Heat Transport (InSight) project, Jet Propulsion Laboratory, California Institute of Technology, under a contract with the National Aeronautics and Space Administration (NASA). The Houston team was partially funded by EAR-1621878. A. Spiga and L. Rolland acknowledge funding by Centre National d’Études Spatiales (CNES). This article constitutes InSight Contribution Number 93.

REFERENCES

Allam, A. A., Y. Ben-Zion, and Z. Peng (2014). Seismic imaging of a bimaterial interface along the Hayward fault, CA, with fault zone head waves and direct P arrivals, *Pure Appl. Geophys.* **171**, no. 11, 2993–3011.

Allam, A. A., V. Schulte-Pelkum, Y. Ben-Zion, C. Tape, N. Ruppert, and Z. E. Ross (2017). Ten kilometer vertical Moho offset and shallow velocity contrast along the Denali fault zone from double-difference tomography, receiver functions, and fault zone head waves, *Tectonophysics* **721**, 56–69.

Banerdt, W. B., S. Smrekar, P. Lognonné, T. Spohn, S. Asmar, D. Banfield, L. Boschi, U. Christensen, V. Dehant, W. M. Folkner, *et al.* (2013). InSight: A Discovery Mission to Explore the Interior of Mars, *44th Lunar Planet. Sci. Conf.*, 1915 pp.

Bayer, B., R. Kind, M. Hoffmann, X. Yuan, and T. Meier (2012). Tracking unilateral earthquake rupture by P-wave polarization analysis, *Geophys. J. Int.* **188**, no. 3, 1141–1153.

Böse, M., J. F. Clinton, S. Ceylan, F. Euchner, M. van Driel, A. Khan, D. Giardini, P. Lognonné, and W. B. Banerdt (2016). A probabilistic framework for single-station location of seismicity on Earth and Mars, *Phys. Earth Planet. In.* **262**, 48–65.

Böse, M., D. Giardini, S. Stähler, S. Ceylan, J. F. Clinton, M. van Driel, A. Khan, F. Euchner, P. Lognonné, and W. B. Banerdt (2018). Magnitude scales for Marsquakes, *Bull. Seismol. Soc. Am.* **108**, no. 5A, 2764–2777.

Ceylan, S., M. van Driel, F. Euchner, A. Khan, J. F. Clinton, L. Krischer, M. Böse, S. C. Stähler, and D. Giardini (2017). From initial models of seismicity, structure and noise to synthetic seismograms for Mars, *Space Sci. Rev.* **211**, nos. 1/4, 595–610.

Clinton, J., D. Giardini, M. Böse, S. Ceylan, M. van Driel, F. Euchner, R. F. Garcia, S. Kedar, A. Khan, S. C. Stähler, *et al.* (2018). The Marsquake service: Securing daily analysis of SEIS data and building the Martian seismicity catalogue for InSight, *Space Sci. Rev.* **214**, no. 8, doi: 10.1007/s11214-018-0567-5.

Clinton, J., D. Giardini, P. Lognonné, B. W. Banerdt, M. van Driel, M. Drilleau, N. Murdoch, M. P. Panning, R. Garcia, D. Mimoun, *et al.* (2017). Preparing for InSight: An invitation to participate in a blind test for Martian seismicity, *Seismol. Res. Lett.* **88**, no. 5, 1290–1302.

Daubar, I., P. Lognonné, N. A. Teanby, K. Miljkovic, J. Stevanović, J. Vaubaillon, B. Kenda, T. Kawamura, J. Clinton, A. Lucas, *et al.* (2018). Impact-seismic investigations of the InSight mission, *Space Sci. Rev.* **214**, no. 8, doi: 10.1007/s11214-018-0562-x.

Eisermann, A. S., A. Ziv, and G. H. Wust-Bloch (2015). Real-time back azimuth for earthquake early warning, *Bull. Seismol. Soc. Am.* **105**, no. 4, 2274–2285.

Fernando, B., M. Tsekhmistrenko, and K. Hosseini (2018). Training Martian seismologists for InSight, *Astron. Geophys.* **59**, no. 5, 5.17–5.21.

Folkner, W. M., V. Dehant, S. Le Maistre, M. Yseboodt, A. Rivoldini, T. Van Hoolst, S. W. Asmar, and M. P. Golombek (2018). The rotation and interior structure experiment on the InSight mission to Mars, *Space Sci. Rev.* **214**, no. 5, doi: 10.1007/s11214-018-0530-5.

Gudkova, T. V., P. Lognonné, and J. Gagnepain-Beyneix (2011). Large impacts detected by the Apollo seismometers: Impactor mass and source cutoff frequency estimations, *Icarus* **211**, no. 2, 1049–1065.

Hammer, C., M. Beyreuther, and M. Ohrnberger (2012). A seismic-event spotting system for volcano fast-response systems, *Bull. Seismol. Soc. Am.* **102**, no. 3, 948–960.

Hammer, C., M. Ohrnberger, and D. Fäh (2013). Classifying seismic waveforms from scratch: A case study in the alpine environment, *Geophys. J. Int.* **192**, no. 1, 425–439.

Jurkevics, A. (1988). Polarization analysis of three-component array data, *Bull. Seismol. Soc. Am.* **78**, no. 5, 1725–1743.

Kenda, B., P. Lognonné, A. Spiga, T. Kawamura, S. Kedar, W. B. Banerdt, R. Lorenz, D. Banfield, and M. Golombek (2017). Modeling of ground deformation and shallow surface waves generated by Martian dust devils and perspectives for near-surface structure inversion, *Space Sci. Rev.* **211**, nos. 1/4, 501–524.

Kennett, B. L., and T. Furumura (2013). High-frequency Po/So guided waves in the oceanic lithosphere: I-long-distance propagation, *Geophys. J. Int.* **195**, no. 3, 1862–1877.

Khan, A., M. van Driel, M. Böse, D. Giardini, S. Ceylan, J. Yan, J. F. Clinton, F. Euchner, P. Lognonné, N. Murdoch, *et al.* (2016).

- Single-station and single-event marsquake location and inversion for structure using synthetic Martian waveforms, *Phys. Earth Planet. In.* **258**, 28–42.
- Knapmeyer, M., J. Oberst, E. Hauber, M. Wählisch, C. Deuchler, and R. Wagner (2006). Working models for spatial distribution and level of Mars' seismicity, *J. Geophys. Res.* **111**, no. E11, E11006, doi: [10.1029/2006JE002708](https://doi.org/10.1029/2006JE002708).
- Knapmeyer-Endrun, B., and C. Hammer (2015). Identification of new events in Apollo 16 lunar seismic data by Hidden Markov Model-based event detection and classification, *J. Geophys. Res. Planets* **120**, no. 10, 1620–1645.
- Krischer, L., T. Megies, R. Barsch, M. Beyreuther, T. Lecocq, C. Caudron, and J. Wassermann (2015). ObsPy: A bridge for seismology into the scientific Python ecosystem, *Comput. Sci. Discov.* **8**, no. 1, 014003.
- Lin, F. C., V. C. Tsai, and B. Schmandt (2014). 3-D crustal structure of the western United States: Application of Rayleigh-wave ellipticity extracted from noise cross-correlations, *Geophys. J. Int.* **198**, no. 2, 656–670.
- Lognonné, P., W. B. Banerdt, D. Giardini, W. T. Pike, U. Christensen, P. Laudet, S. de Raucourt, P. Zweifel, S. Calcutt, M. Bierwirth, et al. (2019). SEIS: Insight's seismic experiment for internal structure of Mars, *Space Sci. Rev.* **215**, no. 1, doi: [10.1007/s11214-018-0574-6](https://doi.org/10.1007/s11214-018-0574-6).
- Mimoun, D., N. Murdoch, P. Lognonné, K. Hurst, W. T. Pike, J. Hurley, T. Nébut, and W. B. Banerdt (2017). The noise model of the SEIS seismometer of the InSight mission to Mars, *Space Sci. Rev.* **211**, nos. 1/4, 383–428.
- Murdoch, N., B. Kenda, T. Kawamura, A. Spiga, P. Lognonné, D. Mimoun, and W. B. Banerdt (2017). Estimations of the seismic pressure noise on Mars determined from large Eddy simulations and demonstration of pressure decorrelation techniques for the InSight mission, *Space Sci. Rev.* **211**, nos. 1/4, 457–483.
- Murdoch, N., D. Mimoun, R. F. Garcia, W. Rapin, T. Kawamura, P. Lognonné, D. Banfield, and W. B. Banerdt (2017). Evaluating the wind-induced mechanical noise on the InSight seismometers, *Space Sci. Rev.* **211**, nos. 1/4, 429–455.
- Nissen-Meyer, T., M. van Driel, S. C. Stähler, K. Hosseini, S. Hempel, L. Auer, A. Colombi, and A. Fournier (2014). AxiSEM: Broadband 3-D seismic wavefields in axisymmetric media, *Solid Earth* **5**, no. 1, 425–445.
- Panning, M., É. Beucler, M. Drilleau, A. Mocquet, P. Lognonné, and W. B. Banerdt (2015). Verifying single-station seismic approaches using Earth-based data: Preparation for data return from the InSight mission to Mars, *Icarus* **248**, 230–242.
- Panning, M., P. Lognonné, W. Bruce Banerdt, R. Garcia, M. Golombek, S. Kedar, B. Knapmeyer-Endrun, A. Mocquet, N. A. Teanby, J. Tromp, et al. (2017). Planned products of the Mars structure service for the InSight mission to Mars, *Space Sci. Rev.* **211**, nos. 1/4, 611–650.
- Plesa, A. C., M. Knapmeyer, M. Golombek, D. Breuer, M. Grott, T. Kawamura, P. Lognonné, N. Tosi, and R. C. Weber (2018). Present-day Mars' seismicity predicted from 3-D thermal evolution models of interior dynamics, *Geophys. Res. Lett.* **45**, no. 6, 2580–2589.
- Rivoldini, A., T. Van Hoolst, O. Verhoeven, A. Mocquet, and V. Dehant (2011). Geodesy constraints on the interior structure and composition of Mars, *Icarus* **213**, no. 2, 451–472.
- Ross, Z. E., and Y. Ben-Zion (2014). Automatic picking of direct P, S seismic phases and fault zone head waves, *Geophys. J. Int.* **199**, no. 1, 368–381.
- Schimmel, M. (1999). Phase cross-correlations: Design, comparisons, and applications, *Bull. Seismol. Soc. Am.* **89**, no. 5, 1366–1378.
- Schimmel, M., E. Stutzmann, F. Ardhuin, and J. Gallart (2011). Polarized Earth's ambient microseismic noise, *Geochem. Geophys. Geosyst.* **12**, no. 7, doi: [10.1029/2011GC003661](https://doi.org/10.1029/2011GC003661).
- Schimmel, M., E. Stutzmann, and J. Gallart (2011). Using instantaneous phase coherence for signal extraction from ambient noise data at a local to a global scale, *Geophys. J. Int.* **184**, no. 1, 494–506.
- Selby, N. D. (2001). Association of Rayleigh waves using backazimuth measurements: Application to test ban verification, *Bull. Seismol. Soc. Am.* **1**, no. 3, 580–593.
- Spiga, A., D. Banfield, N. A. Teanby, F. Forget, A. Lucas, B. Kenda, J. A. Rodriguez Manfredi, R. Widmer-Schmidrig, N. Murdoch, M. T. Lemmon, et al. (2018). Atmospheric science with InSight, *Space Sci. Rev.* **214**, no. 7, doi: [10.1007/s11214-018-0543-0](https://doi.org/10.1007/s11214-018-0543-0).
- Spohn, T., M. Grott, S. E. Smrekar, J. Knollenberg, T. L. Hudson, C. Krause, N. Müller, J. Jänchen, A. Börner, T. Wippermann, et al. (2018). The heat flow and physical properties package (HP³) for the InSight mission, *Space Sci. Rev.* **214**, no. 5, doi: [10.1007/s11214-018-0531-4](https://doi.org/10.1007/s11214-018-0531-4).
- Stähler, S. C., and K. Sigloch (2014). Fully probabilistic seismic source inversion—Part 1: Efficient parameterisation, *Solid Earth* **5**, no. 2, 1055–1069.
- Teanby, N. (2015). Predicted detection rates of regional-scale meteorite impacts on Mars with the InSight short-period seismometer, *Icarus* **256**, 49–62.
- van Driel, M., L. Krischer, S. C. Stähler, K. Hosseini, and T. Nissen-Meyer (2015). Instaseis: Instant global seismograms based on a broadband waveform database, *Solid Earth* **6**, no. 2, 701–717.
- Vidale, J. E. (1986). Complex polarization analysis of particle motion, *Bull. Seismol. Soc. Am.* **76**, no. 5, 1393–1405.
- Wieczorek, M. A., and M. Zuber (2004). Thickness of the Martian crust: Improved constraints from geoid-to-topography ratios, *J. Geophys. Res.* **109**, no. E1, E01009.
- Zharkov, V. N., and T. V. Gudkova (2005). Construction of Martian interior model, *Sol. Syst. Res.* **39**, no. 5, 343–373.
- Zheng, Y., and H. Hu (2017). Nonlinear signal comparison and high-resolution measurement of surface-wave dispersion, *Bull. Seismol. Soc. Am.* **107**, no. 3, 1551–1556.
- Zheng, Y., F. Nimmo, and T. Lay (2015). Seismological implications of a lithospheric low seismic velocity zone in Mars, *Phys. Earth Planet. In.* **240**, 132–141.

Martin van Driel
Savas Ceylan
Domenico Giardini
Maren Böse'
Nienke Brinkman
Amir Khan
Simon Christian Stähler
Institute of Geophysics
ETH Zürich
Sonneggstrasse 5
8092 Zürich, Switzerland
vandriel@erdw.ethz.ch

John Francis Clinton
Fabian Euchner
Conny Hammer
Swiss Seismological Service
ETH Zürich
Sonneggstrasse 5
8092 Zürich, Switzerland

Hector Alemany
David Ambrois
Julien Balestra
Jérôme Chèze
Anne Deschamps
Fabrice Peix

Lucie Rolland
Cédric Twardzik
Université Côte d'Azur
Observatoire de la Côte d'Azur
CNRS, IRD
Géoazur
250 rue Albert Einstein
06560 Valbonne, France

Amir Allam
Department of Geology and Geophysics
University of Utah
Frederick Albert Sutton Building
115 S 1460 E #383
Salt Lake City, Utah 84112 U.S.A.

Bruce Banerdt
Ingrid Daubar
Matthew P. Golombek
Sharon Kedar
Mark P. Panning
Jet Propulsion Laboratory
California Institute of Technology
4800 Oak Grove Drive
Pasadena, California 91109 U.S.A.

Dirk Becker
Titus Casademont
Fabian Dethof
David Essing
Katharina Grunert
Celine Hadziioannou
Isabell Hochfeld
Tabea Kilchling
Sarah Mader²
Lorenz Marten
Franziska Mehrkens
Paul Neumann
Robert Neurath
Christoph Schröer
René Steinmann
Noah Trumpik
Philipp Werdenbach-Jarklowski
Institute of Geophysics
University of Hamburg
Bundesstrasse 55
20146 Hamburg, Germany

Marc S. Boxberg
Manuel Ditz
Andre Lamert
Thomas Möller
Marcel Paffrath
Faculty of Geosciences
Institute of Geology, Mineralogy and Geophysics
Ruhr University Bochum

Universitätsstraße 150
44801 Bochum, Germany

Melanie Drilleau
Balthasar Kenda
Philippe Lognonné
Institut de Physique du Globe de Paris
Sorbonne Paris Cité
Université Paris Diderot
35 rue Hélène Brion
75013 Paris, France

Benjamin Fernando
Thomas Garth
Harriet Godwin
Claudia Haindl
Kasra Hosseini
Alexandre Szenicer
Maria Tsekhmistrenko
Department of Earth Sciences
University of Oxford
South Parks Road
Oxford OX1 3AN, United Kingdom

Raphael Garcia
David Mimoun
Naomi Murdoch
ISAE-SUPAERO
Université de Toulouse, DEOS/ SSPA
10 Avenue Edouard Belin
31400 Toulouse, France

Hao Hu
Jiaxuan Li
Yingcai Zheng
Department of Earth and Atmospheric Sciences
University of Houston
3507 Cullen Boulevard
Room 312
Houston, Texas 77204-5007 U.S.A.

Brigitte Knapmeyer-Endrun³
Max-Planck-Institut für Sonnensystemforschung
Justus-von-Liebig-Weg 3
37077 Göttingen, Germany

Diego Mercerat
CEREMA Méditerranée, project team MOUVGS
500 route des Lucioles
06903 Sophia Antipolis, France

Ludovic Perrin
Centre National d'Etudes Spatiales
18 Avenue Edouard Belin
31400 Toulouse, France

Martin Schimmel
Institut of Earth Sciences Jaume Almera-CSIC
C/Lluís Solé i Sabarís s/n
08028 Barcelona, Spain

Eleonore Stutzmann
Institut de Physique du Globe de Paris
1 rue Jussieu
75252 Paris, Cedex 5, France

Aymeric Spiga
Laboratoire de Météorologie Dynamique (LMD/IPSL)
Sorbonne Université, Centre National de la Recherche
Scientifique
École Polytechnique, École Normale Supérieure
Campus Pierre et Marie Curie
BC99, 4 place Jussieu
75005 Paris, France

Renee Weber
NASA Marshall Space Flight Center
ST13/NSSTC 2047
Huntsville, Alabama 35805 U.S.A.

Shane Zhang
Department of Physics
University of Colorado Boulder
390 UCB
Boulder, Colorado 80309-0390 U.S.A.

Published Online 5 June 2019

¹ Also at Swiss Seismological Service, ETH Zürich, Sonneggstrasse 5, 8092 Zürich, Switzerland.

² Also at Karlsruhe Institute of Technology (KIT), Geophysical Institute, Hertzstraße 16, 76187 Karlsruhe, Germany.

³ Now at Institute of Geology and Mineralogy, University of Cologne, Vinzenz-Pallotti-Straße 26, 51429 Bergisch Gladbach, Germany.